J. Fluid Mech. (2026), *vol.* 1030, A31, doi:10.1017/jfm.2026.11279

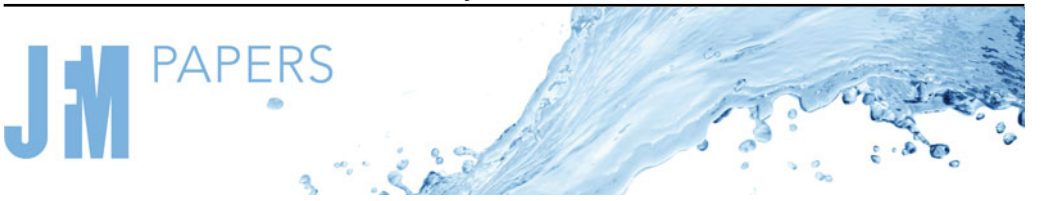

On the angular velocity of a swirling spheroidal squirmer in a viscous fluid

D. Palaniappan[1], **J. Noual**[2] **and H. Nganguia**[2]

[1]Department of Mathematics and Statistics, Texas A&M University–Corpus Christi, Corpus Christi, TX 78412, USA

[2]Department of Mathematics, Towson University, Towson, MD 21252, USA

Corresponding authors: H. Nganguia, hnganguia@towson.edu; D. Palaniappan, devanayagam.palaniappan@tamucc.edu

(Received 23 October 2025; revised 21 January 2026; accepted 1 February 2026)

The propulsion speed of spheroidal squirmers was obtained by Keller & Wu (*J. Fluid Mech.*, 1977, vol. 80, p. A31). It has become the benchmark to investigate the effect of shape on the propulsion of ciliated microorganisms. However, their study focused on translational motion whereas many biologically relevant organisms also experience rotational (or swirling) motion. We derive an analytical expression for the angular velocity of a swirling spheroidal squirmer. Our analysis reveals that spheroidal squirmers rotate faster than their spherical counterparts in Newtonian fluids. We also determine the contribution of the second azimuthal mode to the power dissipation generated by a spheroidal squirmer, and uncover a behaviour uniquely distinct from the power dissipation of a strictly translating swimmer.

Key words: propulsion, swimming/flying, low-Reynolds-number flows

1. Introduction

Following Lighthill and Blake's seminal works on ciliary propulsion of spherical squirmers in a Newtonian fluid (Lighthill 1952; Blake 1971), Keller & Wu (1977) developed theory for the ciliary propulsion of spheroidal squirmers. The original model only included the first swimming mode, and was later extended to include higher modes of the tangential surface velocity (Theers *et al.* 2016; Pohnl, Popescu & Uspal 2020). Nevertheless, similar to the case of spherical squirmers, the translational velocity of the spheroidal squirmers $\boldsymbol{U} = U\boldsymbol{e}_z$, where

$$U = B_1\tau_0\big[\tau_0 - (\tau_0^2 - 1)\,\mathrm{coth}^{-1}\,\tau_0\big], \tag{1.1}$$

depends on the first polar squirming mode B_1. Here, the surface parameter τ_0 is related to the spheroidal squirmer's eccentricity e through $\tau_0 = 1/e$. In the limit $\tau_0 \to \infty$, (1.1) recovers the classical result first obtained by Lighthill (1952) for spherical squirmers. That is, for tangentially actuated spherical squirmers, $U_0 = 2B_1/3$. The translational speed also means that spheroidal, more elongated squirmers propel faster compared with spherical squirmers (as illustrated in figure 1*a*). Equation (1.1) has proven useful, and even critical, in several studies that analytically investigate the influence of shape (through changes in the eccentricity) on the swimming dynamics of spheroidal squirmers in various environments including porous media (Demir *et al.* 2024) and shear-thinning fluids (van Gogh *et al.* 2022).

In addition to translational motion, many microorganisms also undergo rotation. The rotation could be of the entire organism, such as with *Volvox* (Pedley, Brumley & Goldstein 2016), or an extension of the organism's body, such as a flagellum (Purcell 1997). Pak & Lauga (2014) derived swimming kinematics for generalised squirming motion. Besides recovering Lighthill's results for translational motion, they provided analytical expressions for the swirling (or rotational) motion (flow field and velocity) of ciliated microorganisms. In particular, they derived the angular velocity to be

$$\boldsymbol{\Omega}_0 = -\frac{C_{01}}{a^3}\boldsymbol{e}_z, \tag{1.2}$$

where C_{01} is the first azimuthal squirming mode, and a is the squirmer's radius. Two years later, Pedley *et al.* (2016) specifically extended Lighthill and Blake's squirmer model to include axisymmetric swirl velocities.

The angular velocity does not affect the squirming motion in purely viscous fluids (Pak & Lauga 2014). However, recent studies have reported enhancement in the propulsion speed U_0 of spherical squirmers in complex fluids as a result of swirling motion. Specifically, the swirling motion positively influenced the translational speed of spherical squirmers in viscoelastic fluids (Binagia *et al.* 2020; Housiadas, Binagia & Shaqfeh 2021) and shear-thinning fluids (Nganguia *et al.* 2020). In the latter study, the effect of the swirling motion depended on whether the analysis was carried out relative to purely viscous fluids, or exclusively within shear-thinning fluids. A swirling spherical squirmer in shear-thinning fluid did not propel any faster compared with a non-swirling squirmer in a purely viscous fluid. However, when both swimmers are placed in a shear-thinning fluid, swirling squirmers have a distinctive advantage over rotation-free, translating squirmers. Beyond the effects of swirling motion on translational velocity, the angular velocity can be employed to distinguish spherical squirmers in shear-thinning fluids. Nganguia *et al.* (2020) reported that squirmers have distinct rotational direction: positive (negative) rotation for pullers (pushers), and zero rotation for neutral squirmers.

While the swirling motion of spherical squirmers has garnered increasing interest in recent years, the kinematics and energetics of swirling spheroidal squirmers have not been explored nearly as extensively. Indeed, although the rotation of spheroidal rigid bodies has been studied to great extent since the 1910s (Jeffery 1915, 1922; Chwang & Wu 1974), the rotational motion of squirmers has only recently begun to pick the interest of researchers in the field. The available studies have focused on the dynamics and velocity field of the swimmers in purely viscous (Fortune *et al.* 2021; Xia *et al.* 2025*b*) and non-Newtonian fluids (Xia *et al.* 2025*a*).

Fortune *et al.* (2021) used a spheroidal squirmer with axisymmetric swirl as a model for circular mills formed by the marine worm *Symsagittifera roscoffensis* (Franks *et al.* 2016). Specifically, they developed a theoretical framework to describe the flow field generated by the mills. In their study, the dynamics takes place in a purely viscous fluid

where the first azimuthal squirming mode does not contribute to the velocity field. Still in purely viscous fluids, Xia *et al.* (2025*b*) considered the torques experienced by spheroidal squirmers in the absence of azimuthal squirming modes. Here, the torques resulted from the proximity with a wall rather than a self-rotating motion. Later, the authors numerically investigated the dynamics of swirling ellipsoidal squirmers in viscoplastic fluids (Xia *et al.* 2025*a*) and reported significant benefit of the swirling motion on the overall performance of the squirmers. Their analysis did not consider the first azimuthal squirming mode, likely because, as in the case of spherical squirmers, it does not contribute to the flow field. Moreover, the authors only investigated swirling neutral squirmers. This choice may have been guided by the finding that neutral squirmers do not rotate in shear-thinning fluids (Nganguia *et al.* 2020). Nevertheless, the authors' approach did not permit the determination of the angular velocity.

To our knowledge, a result analogous to (1.2) for spheroidal squirmers has yet to be reported in the literature. To address this gap in knowledge, our paper is organised as follows. We formulate the problem in § 2, then derive and discuss results for the velocity field, rotational velocity and power dissipation for a purely rotating spheroidal squirmer in § 3. We conclude with a few remarks on the implication of our work in § 4.

2. Mathematical formulation

2.1. *Geometrical set-up and swirling spheroidal squirmer model*

Given the prolate spheroidal bodies of many ciliates, we employ the prolate spheroidal squirmer for its biological relevance. The prolate spheroidal coordinate system is given by (τ, η, ϕ), where $\tau \geqslant 1$, $-1 \leqslant \eta \leqslant 1$ and $0 \leqslant \phi \leqslant 2\pi$. The position vector

$$\boldsymbol{x} = \frac{c\tau\sqrt{\tau^2-1}}{\sqrt{\tau^2-\eta^2}}\boldsymbol{e}_\tau + \frac{c\eta\sqrt{1-\eta^2}}{\sqrt{\tau^2-\eta^2}}\boldsymbol{e}_\eta, \tag{2.1}$$

where $c = \sqrt{b_z^2 - b_x^2}$ is the semi-focal length of a prolate spheroid with semi-major and semi-minor axes b_z and b_x, respectively. The unit vectors are related to those of the Cartesian coordinates as

$$\boldsymbol{e}_\tau = \frac{\tau\sqrt{1-\eta^2}}{\sqrt{\tau^2-\eta^2}}\boldsymbol{e}_r + \frac{\eta\sqrt{\tau^2-1}}{\sqrt{\tau^2-\eta^2}}\boldsymbol{e}_z, \quad \boldsymbol{e}_\eta = -\frac{\eta\sqrt{\tau^2-1}}{\sqrt{\tau^2-\eta^2}}\boldsymbol{e}_r + \frac{\tau\sqrt{1-\eta^2}}{\sqrt{\tau^2-\eta^2}}\boldsymbol{e}_z, \tag{2.2}$$

where $\boldsymbol{e}_r = \cos\phi\boldsymbol{e}_x + \sin\phi\boldsymbol{e}_y$.

Several swimming mechanisms have been proposed to describe the dynamics of ciliated microorganisms (Lighthill 1952; Ishikawa *et al.* 2020; Rodrigues, Lisicki & Lauga 2021). In this work, we consider the motion of these organisms through a prescribed, constant surface velocity model. While the rotational velocity does not contribute to the overall propulsion of squirmers in purely viscous fluids (Pak & Lauga 2014), it is still associated with the first azimuthal squirming mode. Here, we extend the swirling spheroidal squirmer proposed by Xia *et al.* (2025*a*) by retaining the first azimuthal mode. Thus,

$$\boldsymbol{u}_{sq} = -\tau_0\frac{\sqrt{1-\eta^2}}{\sqrt{\tau_0^2-\eta^2}}\left(C_1 + 3C_2\eta\right)\boldsymbol{e}_\phi, \tag{2.3}$$

where $\tau = \tau_0$ is a parameter denoting the surface of the spheroidal squirmer. Physically, the second azimuthal mode (C_2) describes a rotating flagellum and counter-rotating body. Here, we only keep the first two azimuthal modes due to their physical significance (C_1 is

associated with rotation while C_2 represents rotating flagellum of some microorganisms). For completeness, we present results for the general case of higher azimuthal modes in Appendix A.

2.2. *Governing equations*

We consider a spheroidal squirmer experiencing pure rotation through an axisymmetric flow in an unbounded purely viscous fluid. Given the size of the micro-swimmer, inertial effects can be omitted and the flow field is governed by the incompressible Stokes equation

$$-\boldsymbol{\nabla} p + \mu \nabla^2 \boldsymbol{u} = \boldsymbol{0}, \tag{2.4a}$$

$$\boldsymbol{\nabla} \cdot \boldsymbol{u} = 0, \tag{2.4b}$$

where p is the pressure, μ is the viscosity and $\boldsymbol{u}$ is the fluid velocity. Since the focus of this paper is on the purely rotational motion $\boldsymbol{u} = \langle 0, 0, u_\phi \rangle$ of spheroidal squirmers, the governing equation can be expressed in spheroidal coordinates as $\mu(\nabla^2 \boldsymbol{u})_\phi = 0$, or (Fortune *et al.* 2021)

$$\left(\tau^2 - 1\right)\frac{\partial^2 u_\phi}{\partial \tau^2} + 2\tau \frac{\partial u_\phi}{\partial \tau} - \frac{u_\phi}{\tau^2 - 1} + \left(1 - \eta^2\right)\frac{\partial^2 u_\phi}{\partial \eta^2} - 2\eta \frac{\partial u_\phi}{\partial \eta} - \frac{u_\phi}{1 - \eta^2} = 0. \tag{2.5}$$

In the far field, the velocity in the laboratory frame is given by

$$\boldsymbol{u}(\tau \to \infty, \eta) = \boldsymbol{0}, \tag{2.6}$$

whereas the boundary condition on the squirmer's surface reads

$$\boldsymbol{u}(\tau = \tau_0, \eta) = \boldsymbol{\Omega} \times \boldsymbol{x} + \boldsymbol{u}_{sq}, \tag{2.7}$$

with $\boldsymbol{u}_{sq}$ given by (2.3). The unknown angular velocity $\boldsymbol{\Omega}$ is obtained by enforcing the torque-free condition

$$\int_S \boldsymbol{x} \times (\boldsymbol{\sigma} \cdot \boldsymbol{n})\, \mathrm{d}S = \boldsymbol{0}, \tag{2.8}$$

where S denotes the surface of the squirmer, the stress $\boldsymbol{\sigma} = -p\boldsymbol{I} + \mu \dot{\boldsymbol{\gamma}}$, $\dot{\boldsymbol{\gamma}} = \boldsymbol{\nabla u} + (\boldsymbol{\nabla u})^T$ is the strain tensor and $\boldsymbol{n} = \boldsymbol{e}_\tau$ is the unit normal vector on the squirmer surface. Note that, in the case of a translating spheroidal squirmer, the swimming velocity $\boldsymbol{U}$ (1.1) is derived by enforcing the force-free condition $\int_S \boldsymbol{\sigma} \cdot \boldsymbol{n}\, \mathrm{d}S = \boldsymbol{0}$.

Assuming a squirmer with constant semi-major axis length, we non-dimensionalise lengths using the semi-major axis length b_z, velocities using $b_z C_1$ and pressure using μC_1. In this case, the dimensionless governing equations become

$$-\boldsymbol{\nabla} p + \nabla^2 \boldsymbol{u} = \boldsymbol{0}, \quad \boldsymbol{\nabla} \cdot \boldsymbol{u} = 0, \tag{2.9}$$

while the squirming surface velocity

$$\boldsymbol{u}_{sq} = -\tau_0 \frac{\sqrt{1 - \eta^2}}{\sqrt{\tau_0^2 - \eta^2}} \left(1 + 3\chi_2 \eta\right) \boldsymbol{e}_\phi, \tag{2.10}$$

where $\chi_2 = C_2/(b_z C_1)$. The focal length $c = \sqrt{1 - (b_x/b_z)^2}$. Note that, with this choice of scaling, the equivalent radius for a spherical squirmer is $a = b_z$ and (1.2) becomes $\boldsymbol{\Omega}_0 = \boldsymbol{e}_z$ (after letting $C_{01} = -C_1$). Moreover, in this work the semi-major axis b_z is held fixed, and the focal length can be expressed as $c = 1/\tau_0$.

3. Swirling motion

As done in our previous work (Nganguia & Pak 2018; Demir *et al.* 2024), we exploit the linearity of the Stokes equation and decompose the swirling motion into two separate problems: the pumping problem with velocity $\boldsymbol{u}_P$ and the rotational problem with velocity $\boldsymbol{u}_R$. In the pumping problem, the squirmer is held fixed (by an external force) and not allowed to rotate. A net flow is generated as a result of the prescribed surface velocity on the squirmer. In the rotational problem, the squirmer is allowed to swirl freely with angular velocity $\boldsymbol{\Omega}$. The overall flow field around a swirling squirmer is then the superposition of the solutions of these two problems: $\boldsymbol{u} = \boldsymbol{u}_P + \boldsymbol{u}_R$.

3.1. *Pumping problem*

In this section, the squirmer acts as a pump according to the prescribed surface velocity. The solution of (2.5) (vanishing at infinity) is given by

$$u_\phi = \sum_{n=1}^{\infty} A_n Q_n^1(\cosh\xi) P_n^1(\cos\zeta), \tag{3.1}$$

where P_n^1 and Q_n^1 are the associated Legendre functions of the first and second kind, respectively. Letting $\cosh\xi = \tau$, $\cos\zeta = \eta$, $\sin\zeta = \sqrt{1-\eta^2}$, (3.1) can be re-written as

$$u_\phi(\tau,\eta) = \sum_{n=1}^{\infty} A_n Q_n^1(\tau) P_n^1(\eta). \tag{3.2}$$

We use the boundary condition (2.7) and the orthogonality of the Legendre functions to obtain the constants A_n. This yields

$$A_m = -\frac{\left(m+\frac{1}{2}\right)}{m(m+1)Q_m^1(\tau_0)}\tau_0 \int_{-1}^{1} \left[\frac{\sqrt{1-\eta^2}}{\sqrt{\tau_0^2-\eta^2}}(1+3\chi_2\eta)\right] P_m^1(\eta)\,\mathrm{d}\eta. \tag{3.3}$$

Specifically, for a two-mode squirmer, the coefficients

$$A_1 = \frac{3\tau_0}{4Q_1^1(\tau_0)}\left[\sqrt{\tau_0^2-1} - \left(\tau_0^2-2\right)\csc^{-1}(\tau_0)\right], \tag{3.4a}$$

$$A_2 = \frac{45\tau_0}{12Q_2^1(\tau_0)}\left[\frac{\sqrt{\tau_0^2-1}\left(3\tau_0^2-2\right) + \tau_0^2\left(4-3\tau_0^2\right)\csc^{-1}(\tau_0)}{4}\right]\chi_2, \tag{3.4b}$$

and the velocity field

$$\boldsymbol{u}_P = \left[-A_1 Q_1^1(\tau)\sqrt{1-\eta^2} - 3A_2 Q_2^1(\tau)\eta\sqrt{1-\eta^2}\right]\boldsymbol{e}_\phi. \tag{3.5}$$

It can be shown that the total torque along the swimming direction is $\boldsymbol{M}_P = M_P\boldsymbol{e}_z$, where

$$M_P = 2\pi c^3(\tau_0^2-1)\int_{-1}^{1}\left[\sigma_{\phi\tau}\right]\Big|_{\tau=\tau_0}\sqrt{(\tau_0^2-\eta^2)(1-\eta^2)}\,\mathrm{d}\eta, \tag{3.6}$$

and the stress in the $\boldsymbol{e}_\phi - \boldsymbol{e}_\tau$ plane is given by

$$\sigma_{\phi\tau} = \frac{\sqrt{\tau^2-1}}{c\sqrt{\tau^2-\eta^2}}\frac{\partial u_\phi}{\partial\tau} - \frac{\tau}{c\sqrt{(\tau^2-1)(\tau^2-\eta^2)}}u_\phi. \tag{3.7}$$

Carrying out the integral yields the total torque due to the pumping problem

$$M_P = \frac{16}{3}\pi c^2 A_1, \tag{3.8}$$

where A_1 is given in (3.4*a*).

3.2. *Rotational problem*

We now allow the squirmer to swirl by superposing the solution of the pumping problem with that of the rotation of a rigid spheroidal particle rotating with velocity $\boldsymbol{\Omega}$. In the latter problem, no surface velocity is prescribed. The purely rotational problem was solved by Jeffery (1915, 1922) and Chwang & Wu (1974). The velocity field, given in the polar cylindrical coordinates (r, ϕ, z), is

$$u_\phi = \frac{\beta_0}{c^2 r}\left[(c-z)R_1 + (c+z)R_2 + r^2 \ln\frac{R_1 - (z+c)}{R_2 - (z-c)}\right], \tag{3.9}$$

where

$$\beta_0\left[\frac{2e}{1-e^2} - \ln\left(\frac{1+e}{1-e}\right)\right] = \omega c^2, \tag{3.10a}$$

$$R_1 = \sqrt{(z+c)^2 + r^2}, \tag{3.10b}$$

$$R_2 = \sqrt{(z-c)^2 + r^2}, \tag{3.10c}$$

where e is the eccentricity of the squirmer, and ω is the angular speed. The total torque exerted by the fluid on the prolate spheroid is given by $\boldsymbol{M}_R = -M_R \boldsymbol{e}_z$, where

$$M_R = \frac{32\pi}{3} c\beta_0. \tag{3.11}$$

Noting that the eccentricity $e = 1/\tau_0$ and using the identity $\coth^{-1}(x) = \ln[(x+1)/(x-1)]/2$, the total torque can be expressed in terms of the rotational speed ω from (3.10*a*) as

$$M_R = \frac{16\pi}{3}\frac{\omega c^3(\tau_0^2 - 1)}{\left[\tau_0 - (\tau_0^2 - 1)\coth^{-1}(\tau_0)\right]}. \tag{3.12}$$

Note that, in the spherical limit ($\tau_0 \to \infty$) and for a fixed angular speed, the torque $M_R = 8\pi\omega$, as expected.

The unknown rotational speed ω is obtained by applying the torque-free condition on the squirmer

$$\boldsymbol{M}_P + \boldsymbol{M}_R = \boldsymbol{0}. \tag{3.13}$$

After carrying out the calculation, (3.13) yields

$$\omega = \frac{3\tau_0\left[\sqrt{\tau_0^2 - 1} - (\tau_0^2 - 2)\csc^{-1}(\tau_0)\right]}{4c\sqrt{\tau_0^2 - 1}}. \tag{3.14}$$

In the spherical limit $\tau_0 \to \infty$, $\omega = 1$, which recovers (1.2) (in dimensionless form and after scaling $C_{01} = -C_1$). Figure 1(*b*) shows the rotational speed as a function of the squirmer's eccentricity. The result suggests that more elongated swimmers have faster rotation rate. This monotonic behaviour aligns with the translational speed, as illustrated in figure 1(*a*). Thus a translating and swirling spheroidal squirmer in a Newtonian fluid propels and rotates faster compared with its spherical counterpart.

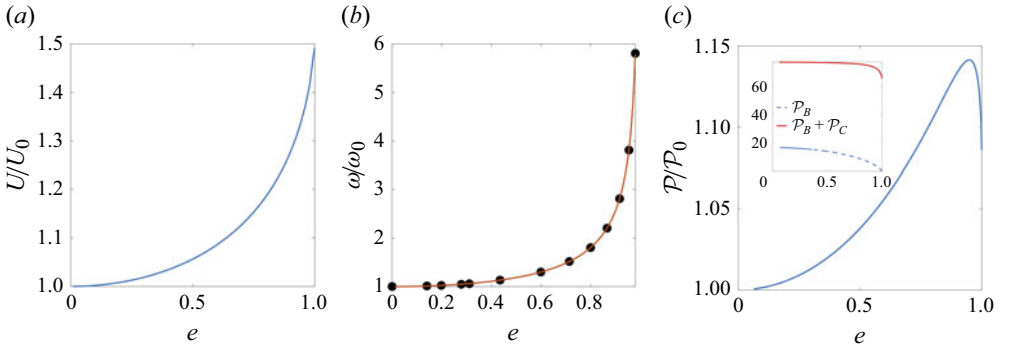

Figure 1. Scaled translational speed U/U_0 (*a*), rotational speed ω/ω_0 (*b*) and power dissipation $\mathcal{P}/\mathcal{P}_0$ (*c*) as a function of the squirmer's eccentricity e. In (*a*), the curve is obtained using (1.1) (Keller & Wu 1977) with $B_1 = 1$. In (*b*), the symbols are obtained from boundary integral simulations whereas the solid curve is calculated using (3.14). In (*c*), the curve is obtained using (3.22) with $\chi_2 = 1$. Inset of (*c*) shows the total power dissipation $P = \mathcal{P}_B + \mathcal{P}_C$ and the power resulting from the polar squirming modes $\mathcal{P}_B$ plotted as a function of the eccentricity. Here, $\mathcal{P}_C = \mathcal{P}$. The dimensionless quantities in the spherical limit are given by $U_0 = 2/3$, $\omega_0 = -1$ and $\mathcal{P}_0 = 96\pi/5$.

We remark that the angular velocity (3.14) is independent of the second azimuthal squirming mode, χ_2. In general, only the first squirming mode contributes to the angular velocity. This is consistent with the angular velocity of a spherical squirmer (Pak & Lauga 2014). To illustrate this point, consider the contribution of the third azimuthal squirming mode. The surface velocity (2.10) now includes the term $-\tau_0(\tau_0^2 - \eta^2)^{-(1/2)}(1-\eta^2)^{(1/2)}\chi_3[16 - 20(1-\eta^2)]/16\boldsymbol{e}_\phi$. In the spherical limit, this term recovers the third azimuthal squirming mode $\chi_3[\sin\theta + 5\sin(3\theta)]/16$. Then, using (3.3) yields a non-zero term associated with the contribution of the third azimuthal mode to the velocity field. However, the surface stress integrates to zero. This confirms that the total torque M_P only depends on the velocity field contribution associated with the first azimuthal mode. Thus, the angular velocity $\boldsymbol{\Omega}$ is only a function of the first azimuthal mode. This finding contrasts with the translational velocity $\boldsymbol{U}$ that was shown to be affected by all the higher, odd polar modes B_{2n+1} (Pohnl *et al.* 2020). However, for spherical swimmers, note that while the third polar squirming mode does not contribute to the translational velocity in Newtonian fluids (Lighthill 1952; Nganguia & Palaniappan 2024), it does induce propulsion in non-Newtonian fluids (Pietrzyk *et al.* 2019; Housiadas 2021).

3.3. *Velocity field*

The velocity field $\boldsymbol{u} = \boldsymbol{u}_R + \boldsymbol{u}_P$. After substituting the position vector in Cartesian coordinates

$$\boldsymbol{x} = c\sqrt{(\tau^2-1)(1-\eta^2)}\left(\cos\phi\boldsymbol{e}_x + \sin\phi\boldsymbol{e}_y\right) + c\tau\eta\boldsymbol{e}_z, \tag{3.15}$$

in (3.9), evaluating the resulting expression at $\tau = \tau_0$ and simplifying, the rotational velocity field obtained by Chwang & Wu (1974) can be expressed in prolate spheroidal coordinates as

$$\boldsymbol{u}_R = \frac{3}{4}\tau_0\sqrt{1-\eta^2}\left[\sqrt{\tau_0^2-1} - \left(\tau_0^2-2\right)\csc^{-1}(\tau_0)\right]\boldsymbol{e}_\phi. \tag{3.16}$$

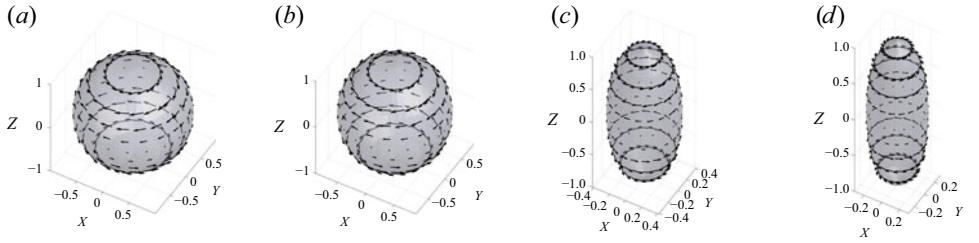

Figure 2. Rotational velocity field $\boldsymbol{v}_{C_2}$ with $\chi_2 = 1$. The surface parameter is (*a*) $\tau_0 = 7.1$, (*b*) $\tau_0 = 2.1$, (*c*) $\tau_0 = 1.1$ and (*d*) $\tau_0 = 1.05$.

On the other end, the pumping velocity can be expressed in the form $\boldsymbol{u}_P = \boldsymbol{u}_{C_1} + \boldsymbol{u}_{C_2}$, where

$$\boldsymbol{u}_{C_1} = -\frac{3}{4}\tau_0\sqrt{1-\eta^2}\left[\sqrt{\tau_0^2-1} - \left(\tau_0^2-2\right)\csc^{-1}(\tau_0)\right]\boldsymbol{e}_\phi, \tag{3.17}$$

and

$$\boldsymbol{u}_{C_2} = \frac{45}{16}\tau_0\eta\sqrt{1-\eta^2}\Big(\left(2-3\tau_0^2\right)\sqrt{\tau_0^2-1} + \left(3\tau_0^2-4\right)\tau_0^2\csc^{-1}(\tau_0)\Big)\chi_2\boldsymbol{e}_\phi. \tag{3.18}$$

With $\eta = \cos\theta$ and lengths scaled by the radius of a spherical squirmer, both (3.16) and (3.17) converge to $\boldsymbol{u}_R = \sin\theta$ and $\boldsymbol{u}_{C_1} = -\sin\theta$ in the spherical limit $\tau_0 \to \infty$. In the same limit, $\boldsymbol{u}_{C_2} = -3\chi_2\sin(2\theta)/2$. This result is consistent with Pak & Lauga (2014) for spherical squirmers. Figure 2 shows the rotational velocity field on the surface of the squirmer that is associated with the second azimuthal mode with $\chi_2 = 1$ for various values of the squirmer's eccentricity (ranging from $\tau_0 = 7.1$ (spherical limit) to $\tau_0 = 1.05$ (needle-like limit)).

3.4. *Power dissipation*

The power dissipation $\mathcal{P} = -\int_S \boldsymbol{\sigma}\cdot\boldsymbol{u}\cdot\boldsymbol{n}\,\mathrm{d}S$. For a spherical squirmer, Pak & Lauga (2014) and Pedley *et al.* (2016) extended the analysis by Lighthill (1952) to include the rate of work for the swirling motion in terms of the swimming azimuthal modes C_n. In dimensionless form, the power dissipation is given by

$$\mathcal{P}_0 = \sum_{n=2}^{\infty}\frac{4n(n+1)(n+2)\pi}{2n+1}\chi_{0n}^2, \tag{3.19}$$

where $\chi_{0n} = C_{0n}/aC_{01}$. In the case of a two-mode squirmer ($n = 2$), (3.19) simplifies to $96\pi\chi_{02}^2/5$. We previously derived the power dissipation of a two-mode prolate spheroidal squirmer in the absence of swirl (Demir *et al.* 2024). Focusing on the azimuthal component in prolate spheroidal coordinates, the power dissipation is given by

$$\mathcal{P} = -2\pi c^2\sqrt{\tau_0^2-1}\int_{-1}^{1}\left(u_\phi\sigma_{\tau\phi}\right)\Big|_{\tau=\tau_0}\sqrt{\tau_0^2-\eta^2}\,\mathrm{d}\eta. \tag{3.20}$$

After carrying out the integral and simplifying, the power dissipation reads

$$\mathcal{P} = -\frac{24\pi c A_2^2}{5\left(\tau_0^2-1\right)}\left[-3\tau_0^2+3\left(\tau_0^2-1\right)\tau_0\coth^{-1}(\tau_0)+2\right] \times\left[-3\tau_0^3+3\left(\tau_0^2-1\right)^2\coth^{-1}(\tau_0)+5\tau_0\right]. \tag{3.21}$$

Then, substituting the coefficient A_2 (3.4b) yields

$$\mathcal{P} = \frac{135\pi c}{d_2}\tau_0^2\left[\left(2-3\tau_0^2\right)\sqrt{\tau_0^2-1}+\left(3\tau_0^2-4\right)\tau_0^2\csc^{-1}(\tau_0)\right]^2 \times\left[\tau_0\left(9\tau_0^4-21\tau_0^2+10\right)+3\left(\tau_0^2-1\right)\coth^{-1}(\tau_0) \times\left(-6\tau_0^4+10\tau_0^2+3\left(\tau_0^2-1\right)^2\tau_0\coth^{-1}(\tau_0)-2\right)\right]\chi_2^2, \tag{3.22}$$

where

$$d_2 = 8\left[6\tau_0^2-6\left(\tau_0^2-1\right)\tau_0\coth^{-1}(\tau_0)-4\right]^2. \tag{3.23}$$

In the spherical limit ($\tau_0\to\infty$), (3.22) yields $\mathcal{P}\to\mathcal{P}_0$. Figure 1(*c*) shows the power dissipation generated by the second azimuthal mode as a function of the squirmer's eccentricity. The power dissipation is scaled by the value of the energy expended by a spherical squirmer. Unlike the monotonically decreasing power dissipation generated from the tangential squirming modes (Demir *et al.* 2024), here, swirling spheroidal squirmers expend more energy compared with spherical squirmers. Of interest is the non-monotonic behaviour of the power, which reaches a maximum $\mathcal{P}/\mathcal{P}_0\approx 1.14$ at high eccentricity ($e\approx 0.95$). In the limit of needle-like shape ($\tau_0\to 1$), the power dissipation $\mathcal{P}=135\pi^3\chi_2^2/64$. It is worth noting that this intriguing behaviour does not alter the conclusion drawn in our previous work (Demir *et al.* 2024); the total power dissipation $P=P_B+P_C$ of a spheroidal squirmer remains lower compared with that of a spherical squirmer (see inset of figure 1*c*).

4. Concluding remarks

In this paper, we derived the rotational velocity (3.14) and power dissipation (3.22) for a swirling spheroidal squirmer in a viscous fluid. Our results show that a spheroidal squirmer always rotates faster than a spherical squirmer (figure 1*b*). Moreover, the contribution of the swirling motion to the power dissipation revealed a non-monotonic behaviour (figure 1*c*), reaching a maximum near the needle-like limit of the eccentricity range.

We make a critical observation for self-propelling, swirling spheroidal squirmers. After close inspection of the total torque M_R, (3.12) can be cast in the form $M_R = 16\pi c^3\alpha\tau_0(\tau_0^2-1)\omega/(3U^*)$, where $\alpha = B_1/b_zC_1$ and $U^*=\alpha\tau_0[\tau_0-(\tau_0^2-1)\coth^{-1}(\tau_0)]$. This shows that the total torque due to the rotational motion is inversely proportional to the translational swimming speed. In fact, we can write $M_R=\tilde{P}_{B_1}/U^*$, where $\tilde{P}_{B_1}$ approximates the mechanical (swimming) power associated with the first polar squirming modes (B_1). The exact expression for the power dissipation associated with the first polar mode is given by $P_{B_1}=-4\pi c(\tau_0^2-1)[\tau_0-(\tau_0^2+1)\coth^{-1}(\tau_0)]$ (Demir *et al.* 2024). In the spherical limit, both expressions recover $16\pi/3$ (Lighthill 1952).

Total viscous power dissipation can be broken down into two parts: external and internal dissipation (Daddi-Moussa-Ider, Goldstein & Vilfan 2023). The former results

from hydrodynamic interaction between the swimmer and the surrounding fluid, while the latter depends on the specific swirling mechanism. For ciliates, internal dissipation is responsible for over 90 % of the total power dissipation (Keller & Wu 1977; Ito, Omori & Ishikawa 2019). Thus, considering different swirling mechanisms such as the one proposed by Ishikawa *et al.* (2020) will yield additional insight into the behaviour reported in figure 1(*c*). We are currently extending the model of Ishikawa *et al.* (2020) to non-spherical squirmers.

Ciliated microorganisms, including *Paramecium*, *Tetrahymena*, etc. move along a helical path. This dynamics is in part due to (i) the rotation of their body on their own major axis or (ii) the rotation of individual cilia (Bullington 1925; Omoto & Kung 1980; Marumo, Yamagishi & Yajima 2021). The biological implications of our findings are twofold. First, similar to (1.1) for the swimming speed (which has been validated against experimental measurements (Rodrigues *et al.* 2021)), (3.14) provides an expression to assess the rate of rotation experienced by ciliated microorganisms. Second, our study also proposes a means to estimate the energy expenditure of swirling spheroidal swimmers.

Our results complement and complete the work by Keller & Wu (1977) by analytically solving the fluid dynamics problem of a rotating spheroidal squirmer in a viscous fluid. Just as the translational velocity has become the benchmark for studying the effect of shape on the dynamics of micro-swimmers in complex fluids, our solution now provides a reference for the rotational velocity of swimmers. For instance, Nganguia *et al.* (2020) showed that spherical pushers and pullers experience opposite, non-zero rotational velocity in shear-thinning fluids. In another study, Binagia *et al.* (2020) and Housiadas *et al.* (2021) reported a marked increase in the propulsion speed of spherical squirmers in viscoelastic fluids. In simpler viscous fluids, asymmetric azimuthal modes resulted in the propulsion of microswimmers along a helical path (Burada, Maity & Julicher 2022). To what extent these conclusions would change when accounting for non-spherical shapes remains unknown. For spheroidal swimmers, we now have an exact analytical expression for the rotational velocity, enabling us to investigate the effect of swirling motion on spheroidal squirmers' kinematics and energetics in complex fluid environments.

Acknowledgements. H.N. thanks Y.-N. Young of the New Jersey Institute of Technology, USA, and H. Shum of the University of Waterloo, Canada, for insightful discussions, and for providing the numerical simulation used to validate the results.

Funding. H. N. gratefully acknowledges funding support from the National Science Foundation grant no. 2211633.

Declaration of interests. The authors report no conflicts of interest.

Appendix A. Coefficients of the flow field in the pumping problem with generalised surface velocity and power dissipation

We aim to derive an expression for the coefficients of the flow field given a generalised surface velocity that accounts for all the azimuthal modes. Note that the surface velocities for polar and azimuthal squirming modes have the same dependence on η. In dimensionless form, they are given by the unique series representation

$$\boldsymbol{u}_{sq} = \tau_0 \sum_{n=1}^{\infty} \frac{P_n^1(\eta)}{\sqrt{\tau_0^2 - \eta^2}} \chi_n. \tag{A1}$$

Applying the boundary condition (2.7) with $\boldsymbol{\Omega} = \mathbf{0}$ (the pumping problem) yields

$$\sum_{n=1}^{\infty} A_n Q_n^1(\tau_0) P_n^1(\eta) = \tau_0 \sum_{n=1}^{\infty} \frac{P_n^1(\eta)}{\sqrt{\tau_0^2 - \eta^2}} \chi_n. \tag{A2}$$

Multiplying both sides by $P_m^1(\eta)$, integrating with respect to $-1 \leqslant \eta \leqslant 1$ and using the the orthogonality property of the associated Legendre polynomials P_m^1 yields

$$A_m = -\frac{\left(m + \frac{1}{2}\right)}{m(m+1)Q_m^1(\tau_0)} \tau_0 \left(\sum_{n=1}^{\infty} \int_{-1}^{1} \frac{P_n^1(\eta) P_m^1(\eta)}{\sqrt{\tau_0^2 - \eta^2}} \, \mathrm{d}\eta \right) \chi_n. \tag{A3}$$

The product of two associated Legendre polynomials can be expressed as the sum over a single associated Legendre polynomial (Dong & Lemus 2002; Pawlak & Stachowiak 2021). The product $P_n^1(\eta) P_m^1(\eta)$ becomes

$$P_n^1(\eta) P_m^1(\eta) = -\sqrt{nm(n+1)(m+1)} \sum_k G P_k(\eta), \tag{A4}$$

where $|n-m| \leqslant k \leqslant n+m$, $k+n+m$ is even, and

$$G = (2k+1) \begin{pmatrix} n & m & k \\ 0 & 0 & 0 \end{pmatrix} \begin{pmatrix} n & m & k \\ -1 & 1 & 0 \end{pmatrix} \tag{A5}$$

is expressed in terms of the $3-j$ symbols $\begin{pmatrix} s_1 & s_2 & s_3 \\ t_1 & t_2 & t_3 \end{pmatrix}$ (Dennis & Walker 1971; Dong & Lemus 2002). Note that the $3-j$ symbol is zero when $k+n+m$ is odd. Moreover,

$$P_k(\eta) = \frac{1}{2^k} \sum_{l=0}^{k/2} (-1)^l \frac{(2k-2l)!}{l!(k-l)!(k-2l)!} \eta^{k-2l}, \tag{A6}$$

and

$$\frac{1}{\sqrt{\tau_0^2 - \eta^2}} = \sum_{j=0}^{\infty} \frac{(2j)!}{4^j (j!)^2} \frac{\eta^{2j}}{\tau_0^{2j+1}}. \tag{A7}$$

Using (A4), (A6) and (A7), the integral

$$\int_{-1}^{1} \frac{P_n^1(\eta) P_m^1(\eta)}{\sqrt{\tau_0^2 - \eta^2}} \, \mathrm{d}\eta = -\sqrt{nm(n+1)(m+1)} \sum_{j=0}^{\infty} \sum_k \sum_{l=0}^{k/2} \frac{(-1)^l (2j)!(2k-2l)!}{2^{2j+k-1}(j!)^2 l!(k-l)!(k-2l)!} \times \frac{G \tau_0^{-(2j+1)}}{k-2l+2j+1}. \tag{A8}$$

Substituting (A8) into (A3) yields the coefficients of the velocity field associated with each azimuthal mode m

$$A_m = \frac{\left(m + \frac{1}{2}\right)}{m(m+1)Q_m^1(\tau_0)} \tau_0 \left(\sum_{n=1}^{\infty} \sum_k \sum_{l=0}^{k/2} \frac{(-1)^l \sqrt{nm(n+1)(m+1)}(2k-2l)!}{2^{k-1} l!(k-l)!(k-2l)!} G \times \sum_{j=0}^{\infty} \frac{(2j)!}{4^j (j!)^2} \frac{1}{(k-2l+2j+1)\tau_0^{2j+1}} \right) \chi_n. \tag{A9}$$

Note that, for $k = 2l$, the summation over j is the series representation of the inverse cosecant function. Moreover, while the coefficients A_m are generally non-zero, the contribution of the higher azimuthal modes to the angular velocity vanishes after applying the torque-free condition.

A general expression for the power dissipation for all azimuthal modes is given by

$$\mathcal{P} = -2\pi c \int_{-1}^{1} \Bigg[\left(\tau_0^2 - 1\right) \sum_{n=2}^{\infty} a_n P_n^1(\eta) \times \sum_{n=2}^{\infty} b_n P_n^1(\eta) - \tau_0 \sum_{n=2}^{\infty} a_n P_n^1(\eta) \times \sum_{n=2}^{\infty} a_n P_n^1(\eta) \Bigg] \mathrm{d}\eta, \tag{A10}$$

where $a_n = A_n Q_n^1(\tau_0)$ and $b_n = A_n Q_n^{1'}(\tau_0)$. Since the associated Legendre polynomial

$$P_n^m(x) = \frac{1}{2^n n!} \left(1 - x^2\right)^{m/2} \frac{\mathrm{d}^{n+m}}{\mathrm{d}x^{n+m}} \left(x^2 - 1\right)^n, \tag{A11}$$

setting $m = 1$, the power dissipation can be re-written as

$$\begin{aligned} \mathcal{P} = -2\pi c \int_{-1}^{1} \Bigg[\left(\tau_0^2 - 1\right) \Bigg(\sum_{n=2}^{\infty} a_n \frac{1}{2^n n!} \frac{\mathrm{d}^{n+1}}{\mathrm{d}\eta^{n+1}} \left(\eta^2 - 1\right)^n \Bigg) \\ \times \Bigg(\sum_{n=2}^{\infty} b_n \frac{1}{2^n n!} \frac{\mathrm{d}^{n+1}}{\mathrm{d}\eta^{n+1}} \left(\eta^2 - 1\right)^n \Bigg) \\ - \tau_0 \Bigg(\sum_{n=2}^{\infty} a_n \frac{1}{2^n n!} \frac{\mathrm{d}^{n+1}}{\mathrm{d}\eta^{n+1}} \left(\eta^2 - 1\right)^n \Bigg)^2 \Bigg] (1 - \eta^2)\, \mathrm{d}\eta. \end{aligned} \tag{A12}$$

When $n = 2$, (A12) recovers (3.22), the contribution of the second azimuthal mode to the power dissipation. In this case, (A12) reduces to

$$\mathcal{P} = -\frac{24\pi c A_2^2}{5} Q_2^1(\tau_0) \Big[\left(\tau_0^2 - 1\right) Q_2^{1'}(\tau_0) - \tau_0 Q_2^1(\tau_0) \Big], \tag{A13}$$

where the coefficient A_2 is given in (3.4b), and the associated Legendre function of the second kind $Q_2^1 = \sqrt{\tau_0^2 - 1}[(3\tau_0^2 - 2)/(\tau_0^2 - 1) - 3\tau_0 \coth^{-1}(\tau_0)]$.

After substituting A_2 and Q_2^1 and simplifying, we recover the contribution of the second azimuthal mode (3.22).

References

Binagia, J.P., Phoa, A., Housiadas, K.D. & Shaqfeh, E.S.G. 2020 Swimming with swirl in a viscoelastic fluid. *J. Fluid Mech.* **900**, A4.

Blake, J.R. 1971 A spherical envelope approach to ciliary propulsion. *J. Fluid Mech.* **46**, 199–208.

Bullington, W.E. 1925 A study of spiral movement in the ciliate Infusoria. *Arch. Protistenk.* **50**, 219–275.

Burada, P.S., Maity, R. & Julicher, F. 2022 Hydrodynamics of chiral squirmers. *Phys. Rev. E* **105**, 024603.

Chwang, A.T. & Wu, T.Y.-T. 1974 Hydromechanics of low-Reynolds-number flow. Part 1. Rotation of axisymmetric prolate bodies. *J. Fluid Mech.* **63**, 607–622.

Daddi-Moussa-Ider, A., Goldstein, R. & Vilfan, A. 2023 Minimum entropy production by microswimmers with internal dissipation. *Nat. Commun.* **14**, 6060.

Demir, E., van Gogh, B., Palaniappan, D. & Nganguia, H. 2024 The effect of particle geometry on squirming in a heterogeneous medium. *J. Fluid Mech.* **986**, A20.

DENNIS, S.C.R. & WALKER, J.D.A. 1971 Calculation of the steady flow past a sphere at low and moderate Reynolds numbers. *J. Fluid Mech.* **48**, 771–789.
DONG, S.-H. & LEMUS, R. 2002 The overlap integral of three associated Legendre polynomials. *Appl. Math. Lett.* **15**, 541–546.
FORTUNE, G.T., WORLEY, A., SENDOVA-FRANKS, A.B., FRANKS, N.R., LEPTOS, K.C., LAUGA, E. & GOLDSTEIN, R.E. 2021 The fluid dynamics of collective vortex structures of plant-animal worms. *J. Fluid Mech.* **914**, A20.
FRANKS, N.R., WORLEY, A., GRANT, K.A.J., GORMAN, A.R., VIZARD, V., PLACKETT, H., DORAN, C., GAMBLE, M.L., STUMPE, M.C. & SENDOVA-FRANKS, A.B. 2016 Social behaviour and collective motion in plant-animal worms. *Proc. R. Soc. B* **283**, 20152946.
VAN GOGH, B., DEMIR, E., PALANIAPPAN, D. & PAK, O.S. 2022 The effect of particle geometry on squirming through a shear-thinning fluid. *J. Fluid Mech.* **938**, A3.
HOUSIADAS, K.D. 2021 An active body in a Phan-Thien and Tanner fluid: the effect of the third polar squirming mode. *Phys. Fluids* **33**, 043110.
HOUSIADAS, K.D., BINAGIA, J.P. & SHAQFEH, E.S.G. 2021 Squirmers with swirl at low Weissenberg number. *J. Fluid Mech.* **911**, A6.
ISHIKAWA, T., PEDLEY, T.J., DRESCHER, K. & GOLDSTEIN, R.E. 2020 Stability of dancing Volvox. *J. Fluid Mech.* **903**, A11.
ITO, H., OMORI, T. & ISHIKAWA, T. 2019 Swimming mediated by ciliary beating: comparison with a squirmer model. *J. Fluid Mech.* **874**, 774–796.
JEFFERY, G.B. 1915 On the steady rotation of a solid of revolution in a viscous fluid. *Proc. Lond. Math. Soc.* **s2_14**, 327–338.
JEFFERY, G.B. 1922 The motion of ellipsoidal particles immersed in a viscous fluid. *Proc. R. Soc. A* **102**, 161–179.
KELLER, S.R. & WU, T.Y. 1977 A porous prolate-spheroidal model for ciliated micro-organisms. *J. Fluid Mech.* **80**, A31.
LIGHTHILL, M.J. 1952 On the squirming motion of nearly spherical deformable bodies through liquids at very small Reynolds number. *Commun. Pure Appl. Math.* **109**, 118.
MARUMO, A., YAMAGISHI, M. & YAJIMA, J. 2021 Three-dimensional tracking of the ciliate Tetrahymena reveals the mechanism of ciliary stroke-driven helical swimming. *Commun. Biol.* **4**, 1209.
NGANGUIA, H. & PAK, O.S. 2018 Squirming motion in a brinkman medium. *J. Fluid Mech.* **855**, 554–573.
NGANGUIA, H. & PALANIAPPAN, D. 2024 Ciliary propulsion through non-uniform flows. *J. Fluid Mech.* **986**, A14.
NGANGUIA, H., ZHENG, K., CHEN, Y., PAK, O.S. & ZHU, L. 2020 A note on a swirling squirmer in a shear-thinning fluid. *Phys. Fluids* **32**, 111906.
OMOTO, C.K. & KUNG, C. 1980 Rotation and twist of the central-pair microtubules in the cilia of Paramecium. *J. Cell Biol.* **87**, 33–46.
PAK, O.S. & LAUGA, E. 2014 Generalized squirming motion of a sphere. *J. Engng Math.* **88**, 1–28.
PAWLAK, M. & STACHOWIAK, M. 2021 Analytical angular solutions for the atom-diatom interaction potential in a basis set of products of two spherical harmonics: two approaches. *J. Math. Chem.* **59**, 2193–2205.
PEDLEY, T.J., BRUMLEY, D.R. & GOLDSTEIN, R.E. 2016 Squirmers with swirl: a model for Volvox swimming. *J. Fluid Mech.* **798**, 165–186.
PIETRZYK, K., NGANGUIA, H., DATT, C., ZHU, L., ELFRING, G.J. & PAK, O.S. 2019 Flow around a squirmer in a shear-thinning fluid. *J. Non-Newtonian Fluid Mech.* **268**, 101–110.
POHNL, R., POPESCU, M.N. & USPAL, W.E. 2020 Axisymmetric spheroidal squirmers and self-diffusiophoretic particles. *J. Phys.: Condens. Matter* **32**, 164001.
PURCELL, E.M. 1997 The efficiency of propulsion by a rotating flagellum. *Proc. Natl Acad. Sci. USA* **94**, 11307–11311.
RODRIGUES, M.F.V., LISICKI, M. & LAUGA, E. 2021 The bank of swimming organisms at the micron scale (BOSO-Micro). *PLoS One* **16**, e0252291.
THEERS, M., WESTPHAL, E., GOMPPER, G. & WINKLER, R.G. 2016 Modeling a spheroidal microswimmer and cooperative swimming in a narrow slit. *Soft Matt.* **12**, 7372.
XIA, Y., YU, Z., LIN, Z. & ISHIKAWA, T. 2025*a* Swimming *a*nd mixing of an ellipsoidal squirmer in a viscoplastic fluid. *J. Fluid Mech.* **1015**, A12.
XIA, Y., YU, Z., ZHANG, M., LIN, Z. & OUYANG, Z. 2025*b* Swimming dynamics of a spheroidal micro swimmer near a wall. *Phys. Rev. E* **111**, 045106.